Development of Path Integral Monte Carlo Simulations with Localized Nodal Surfaces for Second-Row Elements

Burkhard Militzer and Kevin P. Driver

Phys. Rev. Lett. **115**, 176403 — Published 22 October 2015

DOI: 10.1103/PhysRevLett.115.176403

Development of Path Integral Monte Carlo Simulations with Localized Nodal Surfaces for Second-Row Elements

Burkhard Militzer[1, 2] and Kevin P. Driver[1]

[1] *Department of Earth and Planetary Science, University of California, Berkeley*
[2] *Department of Astronomy, University of California, Berkeley*

We extend the applicability range of fermionic path integral Monte Carlo simulations to heavier elements and lower temperatures by introducing various localized nodal surfaces. Hartree-Fock nodes yield the most accurate prediction for pressure and internal energy that we combine with the results from density functional molecular dynamics simulations to obtain a consistent equation of state for hot, dense silicon under plasma conditions and in the regime of warm dense matter ($2.3{-}18.6\ \mathrm{g\,cm^{-3}}$, $5.0\times10^5 - 1.3\times10^8\ \mathrm{K}$). The shock Hugoniot curve is derived and the structure of the fluid is characterized with various pair correlation functions.

PACS numbers: 62.50.-p,31.15.A-,61.20.Ja,64.30.-t

The development of a first-principles methodology for warm dense matter (WDM) applications that treats temperature effects consistently is a key component of the stewardship of plasma science [1, 2]. Indeed, technological progress in high energy density physics (HEDP) applications, such as fusion energy [3, 4], shock-wave physics [5], astrophysical processes [6–8], and planetary [9, 10] and stellar [11] interiors, relies on simulations for input and guidance. WDM is broadly described as the HEDP regime between condensed matter and ideal plasmas, where strong electron correlation and quantum and ionization effects are all important.

For the low temperature part of the WDM regime, density functional molecular dynamics (DFT-MD) [12] is an accurate and efficient first-principles simulation method. The thermal occupation of electronic states is treated as a perturbation of the ground state by Fermi-Dirac smearing [13]. The main drawback of this method is that it becomes computationally infeasible as electrons occupy more bands with increasing temperature. Some alternative DFT-MD-based methods, such as orbital-free DFT [14, 15] and average-atom models [16], have made progress on overcoming the thermal-occupation deficiency, but efforts to improve accuracy are still underway [17, 18].

Here, we focus on the development of the path integral Monte Carlo (PIMC) method [19], which naturally incorporates finite temperature quantum effects by working within the many-body thermal density matrix formalism. The combination with Monte Carlo sampling makes this approach one of the most appropriate first-principles simulation techniques for quantum systems at finite temperature, (T). Since the length of the path scales like $1/T$, the method becomes increasingly efficient for high temperatures. Electrons and nuclei are often treated equally as paths but here we treat the nuclei classically because their zero-point motion is negligible for the temperatures under consideration.

PIMC simulations with more than two electrons in a dense system suffer from a fermion sign problem, which we solve by introducing the the fixed node approximation [20, 21] that restricts paths to remain in the positive regions of a trial density matrix, $\rho_T(\mathbf{R},\mathbf{R}_t;t)>0$. The restricted path integral reads,

$$\rho_F(\mathbf{R},\mathbf{R}';\beta) = \frac{1}{N!}\sum_{\mathcal{P}}(-1)^{\mathcal{P}}\int_{\mathbf{R}\to\mathcal{P}\mathbf{R}',\,\rho_T>0} \mathbf{dR}_t\ \ e^{-S[\mathbf{R}_t]}, \quad (1)$$

where the action, S, weights every path and $\mathcal{P}$ denotes permutations of identical particles. The most common approximation to the trial density matrix is a Slater determinant of single particle density matrices,

$$\rho_T(\mathbf{R},\mathbf{R}';\beta) = \Big|\Big|\rho^{[1]}(r_i,r'_j;\beta)\Big|\Big|_{ij}\ , \quad (2)$$

in combination with the free particle (FP) density matrix,

$$\rho_0^{[1]}(r,r';\beta) = \sum_k e^{-\beta E_k}\,\Psi_k(r)\,\Psi_k^*(r')\quad , \quad (3)$$

derived from a sum over plane waves, $\Psi_k(r)$. The latter is usually converted into Gaussian form [20]. FP nodes becomes exact in the limit of high temperature. Interaction effects have been introduced to the nodal structure on the variational level [22, 23].

In previous work [24–29], we have shown FP nodes can be sufficient to bridge the WDM regime for elements as heavy as neon. FP nodes work for first-row elements because they can still describe the occupation of the 1s state and DFT-MD works well for lower temperatures where the second shell becomes occupied. In order to simulate second-row elements with PIMC, one must go beyond the FP nodal approximation and incorporate the effects of bound states as we describe below in an application to silicon.

We chose to study silicon since it is a natural extension of our original work on carbon and a prototype material with relevance in the semiconductor industry [30], geophysics and planetary science [10], and astrophysics [11, 31–35]. Silicon has a rich solid phase

diagram, displaying 11 solid-state phases under pressure, becoming metallic near 12 GPa [36–38]. A number of dynamic shock compression experiments have been performed [39–45]. Shock-compressed silicon has been studied theoretically with several classical [46–49] and one DFT-MD simulation [50] that investigated pressures up to 500 GPa and temperatures up to 10^4 K. Dynamical properties of shocked silicon plasma states have also been studied extensively by theoretical approaches [51–55].

We perform standard DFT-MD simulations using the VASP code [56]. Supercells with 8 atoms were used for $T \geq 2.5 \times 10^5$ K where the kinetic energy far outweighs the interaction energy, and 24-atoms were used at lower temperatures [29]. Additional details are provided in the supplementary material [57]. For the PIMC calculations, we have used our own code CUPID [61]. The Coulomb interaction is introduced through pair density matrices [62–64]. The nodes are enforced at intervals of 1/8192 Ha, which means we need between 4 and 2560 time slices for simulations in the temperature range of $129 - 1 \times 10^6$ K. It is sufficient to evaluate the pair action only at intervals of 1/1024 Ha [23].

We began our investigation of localized nodal approximations in PIMC with the relatively simple, proof-of-concept problem of computing internal energy and pressure of a stationary silicon atom (one nucleus and 14 electrons) in a periodic cell over a wide temperature range. In Fig. 1, we compared energies from DFT and PIMC using FP nodes, where we found a discrepancy of 5.2 Ha/atom already at 2×10^6 K that increased to 12.6 Ha at 5×10^5 K. We attributed this discrepancy primarily to the FP nodal approximation, which we have shown to work well only as long as the second shell is not significantly occupied [27].

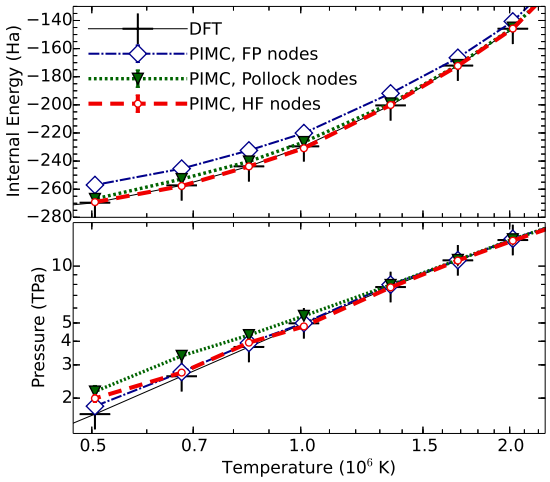

FIG. 1: Internal energy and pressure vs. temperature for a single silicon atom in periodic cell of 5.0 Bohr.

We investigated two approaches to improve upon the FP nodal approximation. First, we added the bound eigenstates of the Coulomb potential of the silicon nuclei, $\Psi_s(r - R_I)$, to the nodal approximation in Eq. 3:

$$\rho^{[1]}(r, r', \beta) = \sum_{I=1}^{N} \sum_{s=0}^{n} e^{-\beta E_s} \Psi_s(r - R_I) \Psi_s^*(r' - R_I) \ , \quad (4)$$

where the number of states, n, needs to be at least 7 in each spin channel in order to provide at least one bound state for every electron. We used the efficient formulation of the Coulomb density matrix put forth in Ref. [62] and hence refer to this approximation as Pollock nodes. The 1s state ($n = 1$) has been added to PIMC nodes once before to simulate dense hydrogen [65]. However agreement with DFT predictions and experimental results was not as good as expected because additional approximations were introduced when the nodes were enforced. Here we enforce the nodes strictly as outlined in Refs. [20, 21].

The adoption of Pollock nodes reduced the energy deviation between DFT and PIMC from 12.6 to 2.7 Ha at 5×10^5 K. However, the pressure deviations increased from 11 to 31% (Fig. 1). We tried to improve upon this result by varying the number of bound states in Eq. 4, testing different time steps, studying various numbers of electrons, and finally by developing a multi-determinental nodal surface in the spirit of quantum chemistry. In the multi-determinantal approach, we adopted a sum of FP fermion determinants where each is added to a different bound shell with the appropriate $e^{-\beta E_s}$ weight. However, this approach did not lead to a significant improvement in the predicted pressure. This discrepancy led us to abandon the Pollock node approximation. We concluded that the eigenstates of non-interacting particles in the Coulomb potential are too confining for interacting electrons.

In our second approach, we constructed a thermal density matrix from Hartree-Fock (HF) orbitals that we computed with the GAMESS code [66] and expanded in a localized basis set (6-31++G). We use again Eq. 4 but this time the functions $\Psi_s(r)$ become the HF orbitals, which are weighted by factors $e^{-\beta E_s}$ where E_s is set to the corresponding HF eigenvalues. Our approach differs from groundstate HF nodes [67]. With our HF nodal approximation, we found perfect agreement with the DFT prediction for the internal energy of the silicon atom over the entire temperature range under consideration (Fig. 1). The resulting PIMC energies are consistently lower than those obtained with other two nodal approximations, which, as illustrate in the supplementary material [57], implies a lower free energy [23] and establishes HF nodes as the most accurate nodes among the three approximations considered here. The PIMC pressures derived with HF nodes agree within the 1 σ error bars for all temperatures of 7×10^5 K and higher. For 5×10^5 K, a small pressure discrepancy remained, but, given the large improvement over FP and Pollock nodes, we decide to adopt HF nodes for our many-particle simulations with

moving nuclei that we discuss for the remainder of this article.

The evaluation of HF orbitals for many moving particles adds a non-negligible burden to computation of the nodes. We vectorized this part of the calculation by evaluating the orbitals for many positions at once. We update the inverse of the determinants whenever possible rather than recomputing it. Nevertheless, when one ion is moved, all determinants need to be re-evaluated, which is not the case for FP nodes that are independent of the ion positions. Despite this additional cost, we were able to perform PIMC simulations with 8 nuclei and 112 electrons for temperatures of 1×10^6 K and above.

We needed to introduce one more methodological development. Upon introducing HF nodes into our simulations with moving nuclei, the acceptance ratio for ion moves rapidly decayed to zero at lower and intermediate temperatures as electron paths began to sample the bound states at the nuclei. Because the nodal surfaces now depend on the nuclear positions, node crossings are almost unavoidable when an ion is moved. The crossing is almost exclusively triggered by nearby electrons. The decay in efficiency was so detrimental that we could not have obtained the smooth $g(r)$ functions in Fig. 2 without the development of multi-particle moves that relocate one nucleus and nearby electrons at once. We needed to design an algorithm that satisfies the detailed balance requirement [19] and does not rely on any permanent pairing of electrons and ions. We introduced a localization function,

$$L_{Ij} = \int_0^\beta dt \; |\Psi_{1s}(r_j(t) - R_I)|^2 \;, \qquad (5)$$

that assigns a probability of finding electron paths, $r_j(t)$, near ion, I. Adopting concepts from the permutation sampling in Ref. [19], we multiply these probabilities to construct a table that contains all moves of one ion with up to four electron paths including those that permute. Because L_{Ij} is a very localized function, the number of significant entries is fairly small so that the table can be constructed efficiently. Once a particular move has be selected from the table, we shift the entire group to a new location within a box of 0.5 Bohr without otherwise changing their paths. This leaves the function L_{Ij} unchanged within the group, which means detailed balance can be satisfied by adopting a particularly simple expression for the acceptance ratio: the sum of table entries for the new location divided by that for the original coordinates. This procedure led to very efficient ion moves. To change internal coordinates of electron paths, we keep relying the on single and multi-electron moves [19].

Figure 3 and supplementary Tab. S1 [57] summarize our equation of state calculations. For density interval of 1 to 8-fold the ambient density of 2.329 g cm^{-3}, PIMC simulations with HF nodes were performed for a temperature range of $129 - 2 \times 10^6$ K and DFT-MD simulations

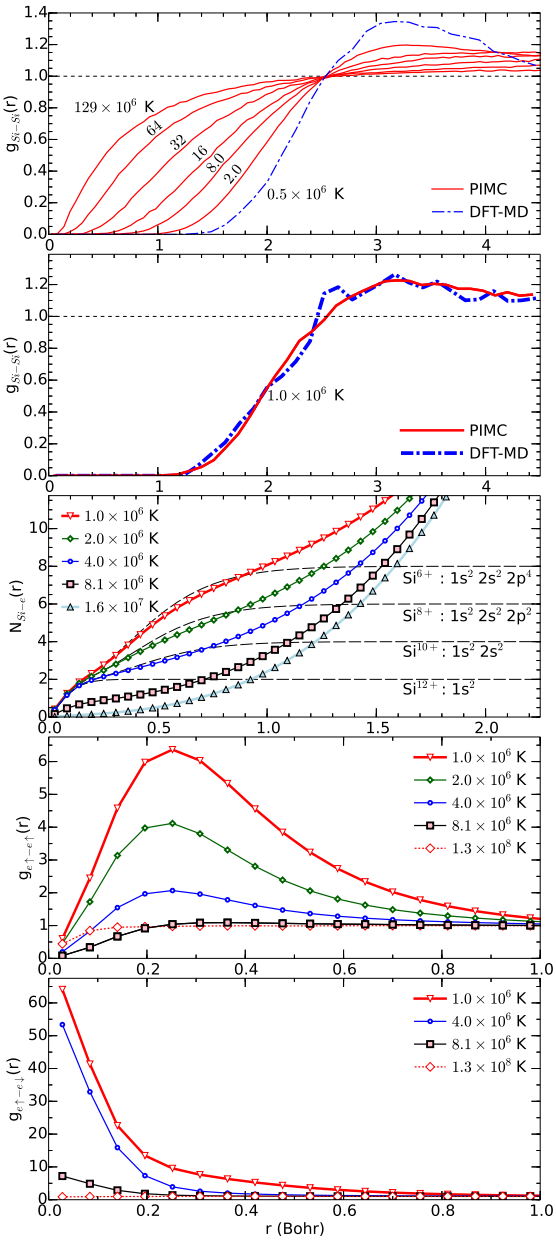

FIG. 2: The top two panels compare the nuclear pair correlation functions from PIMC and DFT-MD at various temperatures. The middle panel shows the integrated nucleus-electron pair correlation function, $N(r)$, computed with PIMC. Results are compared with an isolated ion in order to estimate the ionization state of the plasma. The two lowest panels display the electron-electron pair correlation functions for pairs with parallel and opposite spins. All results are for 4-fold compression.

for $2 - 0.05 \times 10^6$ K. At 2×10^6 K, both methods yield consistent thermodynamic and structural properties despite the fact that both techniques involve very different concepts and approximations. The predicted internal energies deviate by up to 5 Ha/atom and the pressure by up to 4%. A difference of 5 Ha/atom would be equivalent to

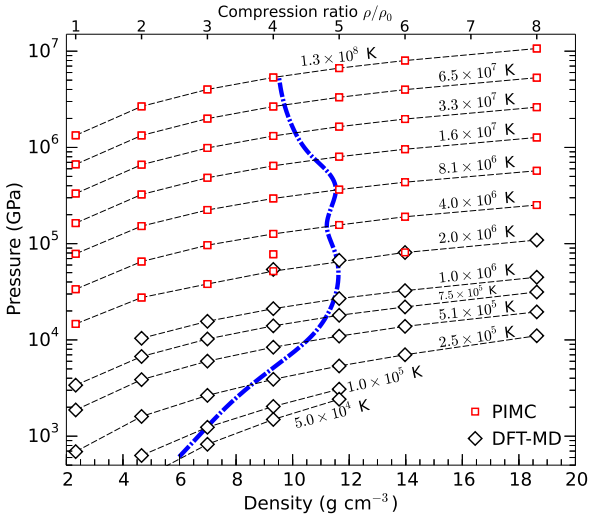

FIG. 3: Pressure-density conditions of our PIMC and DFT-MD simulations. The blue line shows the shock Hugoniot curve.

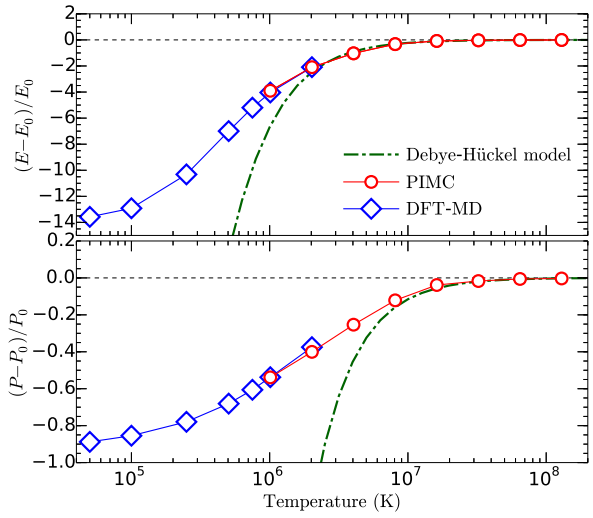

FIG. 4: Internal energy and pressure for a silicon plasma at a density of 9.316 g cm^{-3} are shown versus temperature. We plot the excess quantities relative to a fully ionized noninteracting plasma.

a 2.5% difference in the ionization fraction of the second shell. We attribute these deviations to a combined effect of three approximations: the groundstate DFT exchange-correlation functional, the frozen-core DFT pseudopotential, and our localized nodes in PIMC. While it is difficult to disentangle the errors due to these approximations, we anticipate that the discrepancies will be reduced further when both methods are improved in the future. Figure 4 illustrates that the deviations between PIMC and DFT-MD are small compared to the error in the Debye model. We only plotted excess quantities relative to a fully ionized plasma model because the total internal energy varies by over 10 000 Ha/atom in the parameter range of consideration.

Good agreement between PIMC and DFT-MD is found for the nuclear pair correlation shown in Fig. 2. With PIMC we were also able to derive the integrated nucleus-electron pair correlation function, $N(r)$, that measures how many electron reside on average within a radius, r, from a nucleus. Comparing the information at small r with results for isolated ions, we can estimate the degree of ionization in the plasma. For temperatures of 1, 2, and 4 $\times 10^6$ K, we estimate the average charge of the silicon ions to be +6, +8, and +10 respectively. At higher temperature the 1s states becomes partially ionized also.

The electron-electron pair correlation functions in Fig. 2 yield strong positive correlations, which underlines that multiple electrons are bound to one nucleus. As the temperature is increased, the positive correlation diminishes and eventually even the negative correlations between electrons with parallel spins at small r is reduced.

Finally we derive the principal shock Hugoniot [68]. Under shock compression, a material changes from a initial state with internal energy, pressure, and volume ($E_0 = -289.166$ Ha/atom, P_0=1 bar, V_0 from $\rho_0 = 2.329$ g cm^{-3}) to a final state denoted by (E, P, V) that we can predict theoretically. The shock compression ratio, ρ/ρ_0, is controlled by interaction effects and by excitations of internal degrees of freedom. In Fig. 3, a maximum compression ratio of 4.99 is reached for 1.6×10^6 K where approximately 7 of 14 electrons have been ionized. A second compression maximum of 4.95 is predicted to occur at 8.3×10^6 K, which is caused by the ionization of the 1s state. As we have seen for neon [29], the temperature is too high for this maximum to be studied with DFT-MD. Therefore a combined PIMC and DFT-MD approach is needed to study all features of the principal Hugoniot curve.

By constructing a thermal density matrix with HF orbitals for the purpose of computing fermion nodes, we were able to perform PIMC simulations with heavier elements than was possible before. Through the optimized evaluation of such nodes and the adoption of multi-particle Monte Carlo moves we were able to put together an efficient algorithm and derive the equation of state of silicon plasmas. At lower temperature, we add results from standard DFT-MD simulations. By combining both techniques, we provide a first-principles treatment for all second-row elements in the regime of warm dense matter and for plasma conditions.

This research is supported by DOE (DE-SC0010517). Computational support was provided by NASA, NERSC, and NCAR. B. Austin provided support for reading in the Gamess orbitals. J. Demmel gave advice on the numerics of determinant evaluations.

[1] R. Betti, ed., *Advancing the Science of High Energy Density Laboratory Plasmas* (Office of Fusion Energy Science (OFES)/Fusion Energy Science Advisory Committee (FESAC), Washington D.C., 2009).

[2] R. Rosner, D. Hammer, and T. Rothman, eds., *Basic Research Needs for high energy density laboratory physics* (U.S. Department of Energy, Washington D.C., 2009).

[3] M. K. Matzen, M. A. Sweeney, R. G. Adams, J. R. Asay, J. E. Bailey, G. R. Bennett, D. E. Bliss, D. D. Bloomquist, T. A. Brunner, R. B. Campbell, et al., Phys. Plasmas **12**, 055503 (2005).

[4] I. Cook, Nat. Mater. **5**, 77 (2006).

[5] R. Cauble, D. K. Bradley, P. M. Celliers, G. W. Collins, L. B. D. Siliva, and S. J. Moon, Contrib. Plasma Physics **41**, 239 (2001).

[6] H. M. V. Horn, Science **252**, 384 (1991).

[7] G. Chabrier, F. Douchin, and A. Y. Potekhin, J. Phys.: Condens. Matter **14**, 9133 (2002).

[8] M. Cotelo, P. V. adn A. G. de la Varga, and C. Garcia-Fernandez, Astrophys. Space Sci. **336**, 53 (2011).

[9] J. J. Fortney, S. H. Glenzer, M. Koenig, B. Militzer, D. Saumon, and D. Valencia, Phys. Plasmas **16**, 041003 (2009).

[10] A. Bennuzzi-Mounaix, S. Mazevet, A. Ravasio, T. Vinci, A. Denoeud, M. Koenig, N. Amadou, E. Brambrink, F. Festa, A. Levy, et al., Phys. Scr. **T161**, 014060 (2014).

[11] C. Hansen and S. Kawaler, *Stellar Interiors: Physical Principles, Structure, and Evolution*, vol. 1 of *Astronomy and astrophysics library* (Springer-Verlag New York, 1994).

[12] D. Marx and J. Hutter, Modern methods and algorithms of quantum chemistry **1**, 301 (2000).

[13] M. Verstraete and X. Gonze, Phys. Rev. B **65** (2001).

[14] F. Lambert and J. Clérouin and S. Mazevet, Europhys. Lett. **75**, 681 (2006).

[15] F. Lambert, J. Clérouin, S. Mazevet, and D. Gilles, Contrib. Plasma Phys. **47**, 272 (2007).

[16] B. F. Rozsnyai, High. Energy Dens. Phys. **16** (2014).

[17] V. V. Karasiev, D. Chakraborty, O. A. Shukruto, and S. B. Trickey, Phys. Rev. B **88** (2013).

[18] T. Sjostrom and J. Daligault, Phys. Rev. Lett. **113** (2014).

[19] D. M. Ceperley, Rev. Mod. Phys. **67**, 279 (1995).

[20] D. M. Ceperley, J. Stat. Phys. **63**, 1237 (1991).

[21] D. M. Ceperley, in *Monte Carlo and Molecular Dynamics of Condensed Matter Systems*, edited by E. K. Binder and G. Ciccotti (Editrice Compositori, Bologna, Italy, 1996).

[22] B. Militzer and E. L. Pollock, Phys. Rev. E **61**, 3470 (2000).

[23] B. Militzer and D. M. Ceperley, Phys. Rev. Lett. **85**, 1890 (2000).

[24] B. Militzer, D. M. Ceperley, J. D. Kress, J. D. Johnson, L. A. Collins, and S. Mazevet, Phys. Rev. Lett. **87**, 275502 (2001).

[25] B. Militzer, Phys. Rev. Lett. **97**, 175501 (2006).

[26] B. Militzer, Phys. Rev. B **79**, 155105 (2009).

[27] K. P. Driver and B. Militzer, Phys. Rev. Lett. **108**, 115502 (2012).

[28] L. X. Benedict, K. P. Driver, S. Hamel, B. Militzer, T. Qi, A. A. Correa, A. Saul, and E. Schwegler, Phys. Rev. B **89**, 224109 (2014).

[29] K. P. Driver and B. Militzer, Phys. Rev. B **91**, 045103 (2015).

[30] J. Liu and J. Cao and S. Kaierle, ed., *Deformation behavior of single crystal silicon induced by laser shock peening*, vol. 8796 (American Institute of Physics, 2013).

[31] E. Herbst, T. Millar, S. Wlodek, and D. Bohme, Astron. Astrophys. **222**, 205 (1989).

[32] W. D. Langer and a. E. Glassgold, Astrophys. J. **352**, 123 (1990).

[33] D. D. S. MacKay, Mon. Not. R. Astron. Soc. **274**, 694 (1995).

[34] P. Schilke, C. M. Walmsley, G. Pineau des Forets, and D. R. Flower, Astron. Astrophys. **321**, 293 (1997).

[35] A. P. Jones, A. G. G. M. Tielens, D. J. Hollenbach, and C. F. Mckee, Astrophys. J. **433**, 797 (1994).

[36] A. Mujica and A. Rubio and A. Muñoz, Rev. Mod. Phys. **75**, 863 (2003).

[37] D. Alfè, M. J. Gillan, M. D. Towler, and R. J. Needs, Phys. Rev. B **70**, 214102 (2004).

[38] R. G. Hennig, A. Wadehra, K. P. Driver, W. D. Parker, C. J. Umrigar, and J. W. Wilkins, Phys. Rev. B **82**, 014101 (2010).

[39] P. Celliers, a. Ng, G. Xu, and a. Forsman, Phys. Rev. Lett. **68**, 2305 (1992).

[40] R. R. Alcon and D. L. Robbins and S. A. Sheffield and D. B. Stahl and J. N. Fritz, AIP Conf. Proc. **706**, 651 (1977).

[41] S. Gilev and A. Trubachev, Phys. Status Solidi B Basic Res. **211**, 379 (1999).

[42] S. D. Gilev and a. M. Trubachev, J. Phys. Condens. Matter **16**, 8139 (2004).

[43] T. Löwer, V. Kondrashov, M. Basko, a. Kendl, J. Meyerter Vehn, R. Sigel, and a. Ng, Phys. Rev. Lett. **80**, 4000 (1998).

[44] a. Loveridge-Smith, a. Allen, J. Belak, T. Boehly, a. Hauer, B. Holian, D. Kalantar, G. Kyrala, R. W. Lee, P. Lomdahl, et al., Phys. Rev. Lett. **86**, 2349 (2001).

[45] H. Kishimura, H. Matsumoto, and N. N. Thadhani, J. Phys. Conf. Ser. **215**, 012145 (2010).

[46] G. Mogni, A. Higginbotham, K. Gaál-Nagy, N. Park, and J. S. Wark, Phys. Rev. B **89**, 064104 (2014).

[47] E. J. Reed, AIP Conf. Proc. **620**, 343 (2002).

[48] Z. Li, D. Chen, J. Wang, and L. Shao, J. Appl. Phys. **115**, 143507 (2014).

[49] I. I. Oleynik, S. V. Zybin, M. L. Elert, and C. T. White, AIP Conf. Proc. **845**, 413 (2006).

[50] D. Swift, G. Ackland, a. Hauer, and G. Kyrala, Phys. Rev. B **64**, 214107 (2001).

[51] A. Ng, P. Celliers, G. Xu, and A. Forsman, Phys. Rev. E **52**, 4299 (1995).

[52] M. D. Furnish, N. N. Thadhani, and Y. Horie, eds., *Shock Waves and Plasma Physics* (American Institute of Physics, 2002).

[53] A. Ng, International Journal of Quantum Chemistry **112**, 150 (2011).

[54] J. Vorberger, D. O. Gericke, T. Bornath, and M. Schlanges, Phys. Rev. E **81**, 046404 (2010).

[55] J. Vorberger, Z. Donko, I. M. Tkachenko, and D. O. Gericke, Phys. Rev. Lett. **109**, 225001 (2012).

[56] G. Kresse and J. Furthmüller, Phys. Rev. B **54**, 11169 (1996).

[57] See Supplemental Material [url], which includes Refs. [58-60].

[58] J. P. Perdew, K. Burke, and M. Ernzerhof. *Phys. Rev.*

Lett., 77:3865, 1996.
[59] E. W. Brown, B. K. Clark, J. L. DuBois, and D. M. Ceperley. *Phys. Rev. Lett.*, 110:146405, 2013.
[60] P. E. Blöchl. *Phys. Rev. B*, 50:17953, 1994.
[61] B. Militzer, Ph.D. thesis, University of Illinois at Urbana-Champaign (2000).
[62] E. L. Pollock, Comp. Phys. Comm. **52** , 49 (1988).
[63] V. Natoli and D. M. Ceperley, J. Comp. Phys. **117**, 171 (1995).
[64] B. Militzer and R. L. Graham, Journal of Physics and Chemistry of Solids **67**, 2136 (2006).
[65] S. A. Khairallah and J. Shumway and E. Draeger, available on arXiv:1108.1711.
[66] M.W.Schmidt, K.K.Baldridge, J.A.Boatz, S.T.Elbert, M.S.Gordon, J.J.Jensen, S.Koseki, N.Matsunaga, K.A.Nguyen, S.Su, et al., J. Comput. Chem. **14**, 1347 (1993).
[67] J. Shumway, in *Computer Simulation Studies in Condensed-Matter Physics XVI* (Springer Berlin Heidelberg, 2006), p. 181.
[68] Y. B. Zeldovich and Y. P. Raizer, *Elements of Gasdynamics and the Classical Theory of Shock Waves* (Academic Press, New York, 1968).